Analysis of Complex Hypersonic Flows with Strong Viscous/Inviscid Interaction

G. D. Power* and T. J. Barber†
United Technologies Research Center, East Hartford, Connecticut

Two methods to improve the efficiency of predicting viscous/inviscid interaction in hypersonic flow are examined using an explicit full Navier-Stokes and a parabolized Navier-Stokes procedure. For the first method, a coarse grid full Navier-Stokes result is obtained that resolves the interaction effect of the viscous layer on the inviscid flowfield. In order to enhance the calculation of the surface normal gradients, the results of the coarse grid calculation are then used as initial and boundary conditions for another full Navier-Stokes calculation on a refined grid. Comparisons with benchmark experimental data indicate that this approach yields accurate skin friction and wall heat transfer at a substantially reduced computational cost compared to an initial fine grid calculation. The second method is based on a modification of a parabolized Navier-Stokes procedure to properly include upstream influence effects in the strong interaction region. In this approach, the streamwise pressure gradient term has been modified to account for the propagation of pressure waves within the subsonic layer through a global pressure iteration approach. Using this improved algorithm, good agreement with wall pressure, skin friction, and heat transfer is obtained compared with both experimental data and full Navier-Stokes results. The global pressure iteration scheme demonstrates a considerable reduction in computational time and memory requirements compared to the full Navier-Stokes procedure.

Introduction

THE propulsion system of hypersonic flight vehicles is dominated by complex interactions of multiple shocks with the viscous flow. An understanding of these flows and a determination of performance estimates is an essential element in current scramjet and hypersonic vehicle design efforts. Computational Fluid Dynamics (CFD) is viewed as a primary tool for providing this design information due to the inability of ground-based experimental facilities to simulate these extreme flight conditions. Even though the computational power of computer systems has increased dramatically in the past few years, the time and expense required to use state-of-the-art computational methods is such that three-dimensional, viscous, flowfield computation is still not practical for parametric design applications. Thus, any improvement in the accuracy and efficiency of current methods is of prime importance.

A solution of the full Navier-Stokes (NS) equations can provide a complete description of the flow about a hypersonic vehicle including regions of strong viscous/inviscid interaction. Both explicit[1] and implicit[2] time-marching methods have been shown to provide accurate prediction of flows over a wide Mach number range if the important length scales of the flowfield are resolved. However, as the cell size is decreased in order to capture the small length scales, such as those associated with surface transport properties, the computational efficiency, in terms of CPU and in-core storage requirements, diminishes. Methods to improve the efficiency of these solution algorithms by accelerating convergence to steady state have been reported in the literature, but most of these procedures have not as yet been applied to the prediction of hypersonic flow.

Presented as Paper 87-1189 at the AIAA 19th Fluid Dynamics, Plasma Dynamics, and Lasers Conference, Honolulu, HI, June 8-10, 1987; received Aug. 7, 1987; revision received Feb. 1, 1988.

*Associate Research Engineer. Member AIAA.
†Supervisor, Applied Computational Fluid Dynamics. Member AIAA.

Parabolized Navier-Stokes (PNS) methods[3,4] provide a more efficient alternative to full NS techniques for high Reynolds numbers, supersonic, and hypersonic flows through a single-pass, space-marching technique. The PNS methods assume that the upstream influence (elliptic effect) is negligible. This assumption is reasonable over a large portion of the flow due to the dominant influence of the hyperbolic inviscid region and the parabolic boundary layer; however, in the vicinity of shock/boundary-layer interactions, upstream influence is a dominant feature in determining the flow structure. The PNS solution algorithms have been modified previously for low supersonic flows, resulting in Reduced Navier-Stokes (RNS) methods,[5] which address the issue of upstream propagation of information by appropriately differencing the streamwise pressure gradient in the subsonic region of the boundary layer and globally iterating on the pressure field.

The goals of the present study are to examine the unique physical aspects of hypersonic viscous/inviscid interactions and to assess the procedures for accurately predicting these flows through comparison with benchmark experimental data. Procedures are explored for improving the accuracy and efficiency of these solution methods. The efficiency of a NS algorithm is improved by solving the flowfield on a coarse mesh and then using these results as initial and boundary conditions for a calculation on a refined grid in order to enhance the resolution of surface transport properties. The applicability of PNS methods to predict flows with strong viscous/inviscid interaction is addressed by applying an RNS procedure in a hypersonic environment.

Flow Physics

There are many unique features associated with hypersonic flow. These features include real gas effects, extensive transitional boundary-layer regions, three-dimensional shock structures, and complicated viscous/inviscid interaction. For many of these features, improved physical models can and have been developed and incorporated into CFD codes. In this paper, we will concentrate on the prediction of viscous/inviscid interactions that pertain to the coupling effects of the inner viscous shear layer and the outer inviscid flow, particularly shock/boundary-layer interaction.

One important feature of viscous/inviscid interaction in hypersonic flows is the density increase across a shock that forces the boundary layer to thin, inducing an increase in skin friction and heat transfer. Calculations in the results section of this paper will show that the boundary-layer thickness decreases by as much as a factor of 10 just downstream of the interaction region. Thus, resolution of the boundary layer and, in particular, the surface gradients becomes a real issue.

A second feature, termed upstream influence, is characterized by a more global interaction effect such that the conditions at one location in the flowfield are affected by the conditions downstream of that location. The extent of the upstream influence induced by a disturbance can be determined approximately by the infinite Reynolds number analysis known as triple-deck,[6] but no theoretical analysis exists to determine the extent of the streamwise interaction, particularly if separation is present in the interaction region. One explanation for the phenomena of upstream influence is that strong disturbances produced by compression ramps and incident shock waves induce pressure waves that travel upstream through the subsonic portion of the boundary layer, producing a pressure gradient upstream of the actual disturbance. This adverse pressure gradient induces a decrease in the skin friction, an increase in the displacement thickness, and, consequently, a decrease in heat transfer.

A schematic of two typical hypersonic strong viscous/inviscid interactions with separation is shown in Fig. 1. The compression induced by either the ramp or the impinging shock produces a separation zone upstream of the shock. A compression fan is generated in the separation zone and proceeds downstream, eventually intersecting the resultant shock. The boundary layer initially thickens in the recirculating region and then thins dramatically downstream of the shock due to the density increase produced by the compression. The intersection of the leading-edge shock with the ramp shock produces an expansion fan and a contact surface downstream of the intersection. The next section will highlight computational procedures to capture the flow features associated with strong viscous/inviscid interactions of this type.

Analysis

The classical approach toward conventional vehicle analysis has been to use an elementary boundary-layer analysis coupled to an inviscid outer-flow analysis. This method requires little computational effort or storage but can be applied only to weak interaction regions in which the inviscid flow is not significantly affected by the boundary layer. The effects of upstream influence can be predicted by using interacting boundary-layer analyses[7] in which the inviscid flow is allowed to adjust to changes in the displacement thickness and vice versa. However, all boundary-layer methods have limited applicability as tools for predicting hypersonic flows due to the variation of total pressure at the boundary-layer edge, entropy swallowing, and nonzero normal pressure gradients within the boundary layer.

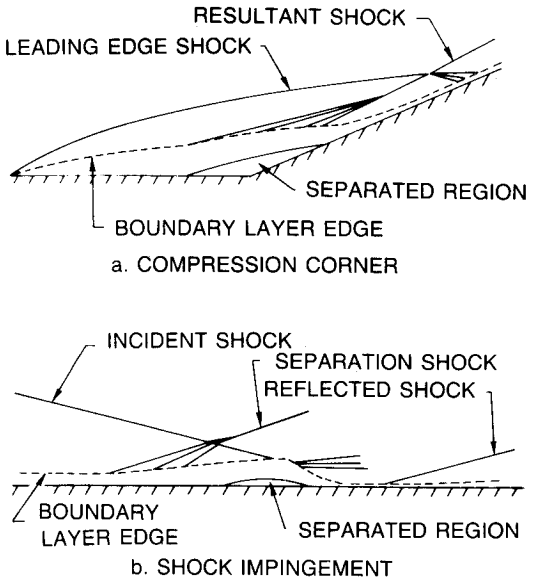

Fig. 1 Typical hypersonic viscous/inviscid interactions.

The most general set of equations for solving hypersonic flowfields are the full NS equations. If the flow is a continuum and appropriate models for molecular and turbulent viscosity as well as for the thermodynamics are used, these equations provide an accurate description of the flowfield. There exists in the literature a number of solution methods using either explicit or implicit time-marching algorithms. Explicit algorithms[1] provide rapid computation at each time level, take full advantage of the vector and parallel computer architectures currently available, and are easily modified for specific applications. Their disadvantage is that the conditional stability limitations on the iteration time step can slow the computation considerably. On the other hand, the time-step limitations on implicit schemes[2] are much less restrictive. However, the iterative inversion of large matrices requires more computational effort per time step than for explicit schemes, most inversion methods are not readily vectorized, and new flow modeling modifications are frequently difficult to incorporate.

For the present study, a robust, explicit, time-marching, shock-capturing scheme based on the 1969 MacCormack algorithm[1] and known as the NASCRIN code[8] was used. The equations are written in strong conservation form in a curvilinear nonorthogonal coordinate system that allows mesh stretching in both the axial and vertical directions. The mesh distribution in the vertical direction is specified according to either the logarithmic compression function of Roberts[9] or any user-specified distribution. For a stretched mesh, the degree of stretching is controlled by a parameter β, where values of β approaching one result in a greater concentration of grid points near the wall. Sutherland's viscosity-temperature law is applied for the calculation of laminar viscosity, while the turbulent viscosity is calculated from a version of the Baldwin-Lomax turbulence model. This solution procedure for the NS equations and others like it have been extensively applied to internal and external problems for a wide range of Mach numbers and flow conditions.

The full NS equations are applicable to a large class of flow problems, but at a high cost, in both computational time and in-core storage requirements. The less complex PNS analyses[3,4] treat a composite set of equations that are applicable in the viscous and inviscid flow. The PNS equations are essentially the NS equations with the streamwise diffusion terms neglected. The term "parabolic" is somewhat misleading, since the differential equations are boundary value, not initial value, in nature. This property must be suppressed numerically in order to march in space by eliminating the occurrence of branching (departure) solutions[5] that manifest themselves through an exponential growth of the solution. The physical reasoning behind numerically suppressing branching and allowing the solution to march in a parabolic fashion is that in most regions of the flow, upstream influence is negligible, i.e., the flow is dominated by both the hyperbolic nature of the inviscid flow and the parabolic nature of the boundary layer. Commonly applied methods to suppress branching include the sublayer approximation of Schiff and Steger,[3] in which the pressure gradient normal to the surface is assumed to be zero across the subsonic layer, and the Vigneron technique,[4] in which the contribution of the streamwise pressure gradient is decreased across the subsonic layer as a function of Mach number based on stability considerations. As a consequence of the space-marching approach, the prediction of upstream influence (hence strong streamwise interaction) is excluded.

The PNS analysis applied in this study is the SCRAMP code,[10] which is based on the Schiff and Steger approach and

represents a two-dimensional PNS analysis that has been extensively used for the prediction of hypersonic flows. The procedure is first-order-accurate in the marching direction and second-order-accurate in the normal direction, with shock fitting outer boundary conditions. The mesh distribution in the vertical direction also is stretched according to the logarithmic distribution of Roberts.[9] Gas properties and laminar transport properties are calculated either from a calorically perfect model or from an equilibrium gas model based on Tannehill and Mugge.[11] The solution is marched implicitly from an initial solution provided by a viscous shock-layer (VSL) analysis or a similar procedure. Since this analysis is a marching scheme and only two planes of data are required, the computational time and in-core storage requirements are quite reasonable.

The NS equations can be used to predict viscous/inviscid interactions, provided there is enough storage and computational time to accurately resolve the multiple length scales and phenomena that occur. In strong streamwise interaction, length scales include the geometric length, the shock-layer thickness, the boundary-layer thickness, the length of the separation bubble, and the strong interaction length scale, which is defined as the distance upstream of a disturbance at which the disturbance is first detected. The various phenomena are the leading-edge shock, the incident shock, the reflected shock, the ramp shock, the separation shock, the separation bubble, the temperature gradients, and the velocity gradients. It is difficult to simultaneously resolve all the length scales associated with the important phenomena. One approach to resolving the small length associated with surface transport properties is to cluster the mesh near the wall, but the decrease in cell size forces smaller time steps and, subsequently, higher computational costs. In addition, refining the mesh near the wall does not necessarily improve the predictive capability of the analysis if the resolution in the inviscid flow suffers as a consequence.

In the present study, two methods have been pursued to improve the efficiency and accuracy of the computational techniques cited in the previous section. The first method is applicable to flows with a large disparity in length scales, such as hypersonic flows, where resolution of the small scales may be important but time consuming to calculate. Here, a primary solution is obtained using the full NS equations on a grid that is sufficiently dense to resolve the displacement interaction effects without necessarily resolving the surface normal gradients. Then the converged solution is applied as an initial solution and as boundary conditions for a separate ex post facto computation on a refined grid to locally enhance the prediction of the surface transport properties. Since the smallest cell sizes occur on the enhanced grid, which is embedded within the primary grid, the time (iterations) required for numerical errors to pass out of the refined grid is much less than it would be for a calculation on a single grid, which fully resolves all phenomena and length scales simultaneously. The mass, momentum, and energy fluxes are applied as boundary conditions at the inflow to the refined grid and along the outer boundary, with no-slip and temperature specified along the wall boundary.

This method is similar to the weak interaction technique in which the outer flow is calculated with an inviscid method and the surface normal gradients are calculated using a boundary-layer analysis. In the present method, the outer flow is calculated with a full NS method in order to properly account for the strong viscous/inviscid interaction, and the surface normal gradients are calculated during a second NS calculation on a refined grid, which locally enhances the accuracy in the near-wall region. The NS equations are used in the local enhancement calculation rather than the boundary-layer equations, since flow reversal and nonzero normal pressure gradients are often present. This method should not be confused with patched or overlapping grid techniques[12,13] that are used to resolve complex geometrical problems. In this case, the calculations are performed separately, not simultaneously, on both grids in order to improve the accuracy of the calculation without incurring the time penalties associated with small cell sizes during the primary calculation.

Even using methods such as the one described, the solution of the full NS equations still can be quite expensive. While the PNS methods provide an efficient alternative to NS solution schemes, the assumption of negligible upstream influence restricts accurate prediction to regions in which weak streamwise interaction is dominant. Near shock/boundary-layer interactions, PNS analyses predict a sharp pressure rise and skin-friction rise downstream of the shock due to the thinning of the boundary layer without the correct behavior upstream of the disturbance. The flowfield prediction becomes even less accurate if separation occurs, and, in fact, these analyses do not predict shock-induced separation at all.

The second approach for improving the current solution methods is based on a modified scheme for solving the PNS equations, referred to as a RNS method. The primary difference between the RNS and PNS approaches is that a mechanism for information to propagate upstream is incorporated into the RNS technique. The pressure relaxation scheme of Barnett and Davis[5] was updated for hypersonic flow and incorporated into the SCRAMP PNS procedure by Barnett and Power.[14] The reader is referred to this paper for details of the method, which will be described briefly. The streamwise pressure gradient in the axial momentum equation is split into two parts: a backward-difference portion similar to the single-pass PNS approach, and a forward-difference portion to allow a mechanism for upstream propagation of information. A splitting parameter ω is used to weight each part as shown:

$$\frac{\partial p}{\partial x} = \omega\left(\frac{\partial p}{\partial x}\right)_b + (1-\omega)\left(\frac{\partial p}{\partial x}\right)_f$$

where the b and f subscripts refer to backward and forward differencing, respectively. The pressure gradient, therefore, changes from a totally backward-differenced form in the supersonic flow to a totally forward-differenced form in the subsonic wall region through specification of the splitting parameter. The pressure field and the Jacobians of the mesh are saved at each global sweep to provide the values at the downstream station, which is lagged in a Gauss-Seidel iteration procedure. Since only two variables are saved, storage requirements are still quite reasonable as compared to full NS procedures. For flows without strong streamwise interaction, the calculation converges in one iteration, whereas for flows with strong streamwise interaction, the convergence rate is related to the axial extent of the interaction region. For most hypersonic flows, the interaction region is confined to the immediate vicinity of the disturbance; therefore, computational effort is minimal.

Results and Discussion

For the purposes of this study, the flat plate/compression ramp data of Holden and Moselle[15] was chosen for comparison. These same data have been used previously as a computational benchmark by other investigators, including Hung and MacCormack[16] and Lawrence et al.[17] The dominant flow feature of the experimental configurations is a single-ramp compression shock. The flow is known to be laminar, thus eliminating the uncertainty of turbulence modeling, and the conditions are such that the perfect gas assumption is sufficient to describe the thermodynamics. Accurate pressure, skin-friction, and heat-transfer data are available for fully evaluating the sensitivity of the computations to the grid and solution scheme. The heat-transfer measurements, taken on an insulated plate using 0.01-in. thin film gages with 1-μs response, were used to verify the laminar nature of the flow.

The configuration geometry analyzed in this study is a two-dimensional, sharp flat plate/compression ramp combination

in a Mach 14.1 flow at a Reynolds number of 1.04×10^5 based on the flat plate length of 0.439 m. The ramp angle was varied in the experiment to change the strength of the ramp shock and hence the extent of viscous/inviscid interaction. Two specific cases at ramp angles of 15 and 24 deg are discussed. The flow over the 15-deg ramp configuration remained attached but did demonstrate some upstream influence effects, while the experimental results for the 24-deg configuration indicate the existence of a large separation region extending upstream of the corner.

Two aspects of the computation will be detailed. The first is the importance of resolving all of the flow features, i.e., the effect of grid on the NS solutions and the role of the local enhancement approach in improving the prediction of normal gradients at the wall. The second aspect is the ramification of including or neglecting the effect of upstream influence in strong streamwise interaction regions. This latter study considers the differences between PNS, RNS, and NS solution procedures.

Flowfield Resolution

The results described hereafter were obtained using the explicit shock-capturing NS procedure (NASCRIN) with 100 points across the flow and 100 points in the axial direction. In the axial direction, the grid was clustered near the leading edge and near the compression corner. All calculations were performed with the minimum numerical smoothing that would allow stable time marching. For most cases, the fourth-order smoothing parameter based on pressure was set to 1.5, while the fourth-order smoothing parameter based on temperature was set to zero. Convergence to steady state was determined for the various calculations initially by monitoring the density residuals. It was found that this parameter did not fully represent a converged solution, and a larger time for convergence based on the number of time steps required for a disturbance to pass four times through the flowfield was subsequently used.

Figure 2 is a plot of the pressure contours for three 15-deg ramp calculations compared with a Schlieren photograph from the experiment.[15] The first NS case was calculated using an evenly spaced mesh in the direction normal to the incoming flow. The results for the second case were obtained on a grid with the same number of points but clustered near the wall using a stretching factor β of 1.2. The final pressure contour plot corresponds to a calculation on a more highly stretched grid generated with a stretching factor of 1.1. The number of time steps to reach steady state were 33,500, 49,500, and 64,000 for the uniform grid and the grids generated using $\beta = 1.2$ and 1.1, respectively. Since the time step is proportional to the size of the smallest mesh element, the number of time steps required to reach steady state increases as the stretching factor approaches 1.0. Furthermore, since the total number of grid points is held constant, the resolution in the inviscid region decreases as the mesh is more highly stretched. The results shown in Fig. 2 indicate that the location of the leading-edge shock varies considerably with grid distribution, and since a large portion of the flowfield is still in the strong normal interaction regime of the leading edge ($\bar{\chi} \cong 8$ at the corner), the predicted leading-edge shock location and strength can significantly affect the solution.

Figure 3 shows a plot of the calculated wall pressure distribution for the three different meshes compared to experimental data. The axes have been nondimensionalized by the freestream pressure p_∞ and the length L of the flat plate. The initial decay in calculated pressure corresponds to the leading-edge interaction effect. The subsequent pressure rise on the ramp is due to the induced corner shock. The intersection of the leading edge and compression shock waves shown in the previous figure induces an expansion fan that results in a decrease in pressure downstream of the intersection. Upstream of the corner, the results obtained on the stretched grids compare well with the data, since the flow in this region is boundary-layer controlled and a stretched mesh best captures this behavior. The resolution of the outer flowfield, as shown in Fig. 2, is strongly dependent on the mesh distribution, and this dependence is reflected in the surface pressure distributions shown in Fig. 3. Increasing the mesh stretching from a uniform grid to a grid with $\beta = 1.2$ moves the predicted pressure on the ramp closer to the data. However, further resolution of the boundary layer ($\beta = 1.1$) results in an overprediction of the pressure levels, indicating that the resolution in the inviscid flow becomes insufficient as more points are moved toward the solid surface.

Figure 4 shows a plot of the skin friction as calculated on each of the grids compared with the experimental data. The results obtained on the uniform grid are poor along the entire surface of the configuration, while both stretched grids compare well with the data over the flat plate region. Due to the thin boundary layer downstream of the ramp shock, the best predictions are obtained on the grid with the most resolution near the wall. Therefore, it is clear that one must simultaneously resolve the outer inviscid and inner viscous

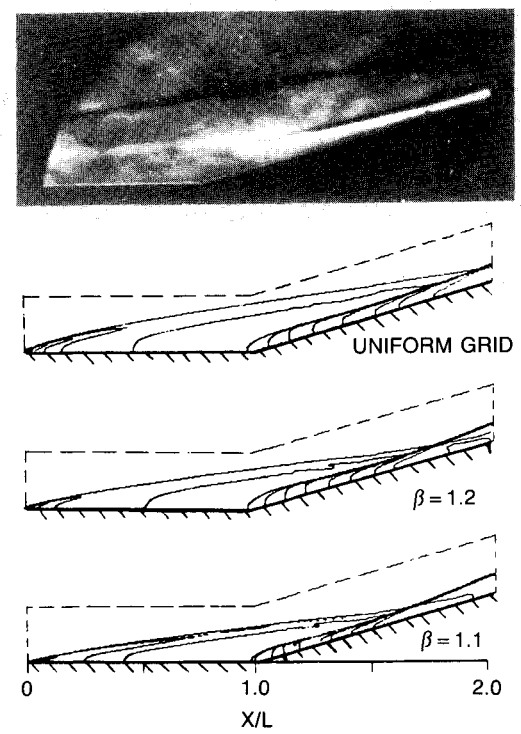

Fig. 2 Effect of grid on calculated pressure contours for 15-deg case.

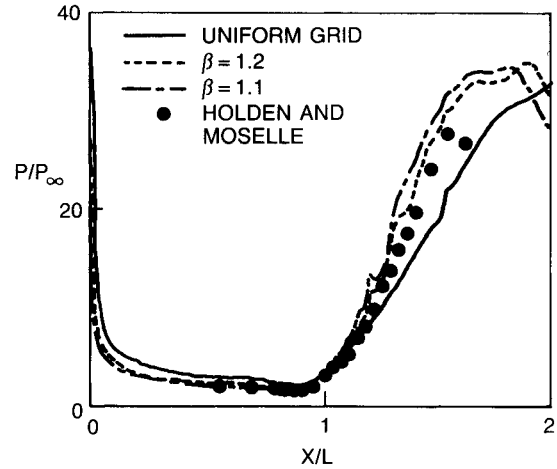

Fig. 3 Effect of grid on calculated wall pressure distribution for 15-deg case.

flowfields in order to properly model the strong coupling between the viscous and inviscid flows.

Calculations have also been made for a ramp angle of 24 deg, in which the ramp shock is much stronger compared to that of the 15-deg case, and therefore the boundary layer is thinner downstream of the shock. As a consequence, resolution of the wall gradients requires even more points near the wall. Figure 5 shows the wall pressure distributions calculated from two NS calculations compared with the experimental data. The grid was evenly spaced for the first calculation, while a stretched grid with $\beta = 1.1$ was used for the second calculation. The number of time steps required to reach steady state were 39,000 and 94,000, respectively. The separation zone is indicated by the pressure plateau starting at $X/L \cong 0.75$. Although the predicted onset of separation, as indicated by this plateau, does not agree precisely with the data, the magnitude and exent of the pressure plateau is predicted well by the results on either grid. In addition, the magnitude of the pressure rise due to the ramp shock is in agreement with the data, although the location of the pressure peak is predicted to be somewhat upstream of the measured location.

The Stanton number distributions are shown in Fig. 6 for both cases compared with the data. The prediction on the flat plate portion is in agreement with the data for both grids. The strong 24-deg ramp shock produces an extremely thin boundary layer downstream of the corner, resulting in a sharp rise in measured heat transfer. In fact, the ratio of boundary-layer thickness upstream of the interaction region compared to the thickness downstream of this region is almost 11. The grids used for these calculations have insufficient definition to resolve the thin boundary layer and, therefore, are unable to accurately simulate the measured heat-transfer levels downstream of the shock, as shown in Fig. 6.

To provide better resolution, points could be redistributed from the inviscid region of the flow to the near-wall region. However, computations showed that this grid redistribution leads to less accurate pressure predictions typical of those shown for the 15-deg case, and run times increase substantially as the cell sizes near the wall decrease. The local enhancement approach discussed in the analysis section was applied to the 24-deg ramp case to determine if an improvement in the prediction of heat transfer could be realized with a minimum of computational effort. In this case, the stretched grid solution was used as the primary solution. However, since the pressure distributions are nearly identical, either solution would be appropriate as the starting point. The outer boundary of the refined grid was chosen outside of the boundary layer but inside the shock layer, and the inflow boundary was chosen upstream of the separation region. A 100×100 grid was constructed for the local enhancement solution, with a stretching factor of 1.1. The solution was iterated for 30,000 time steps.

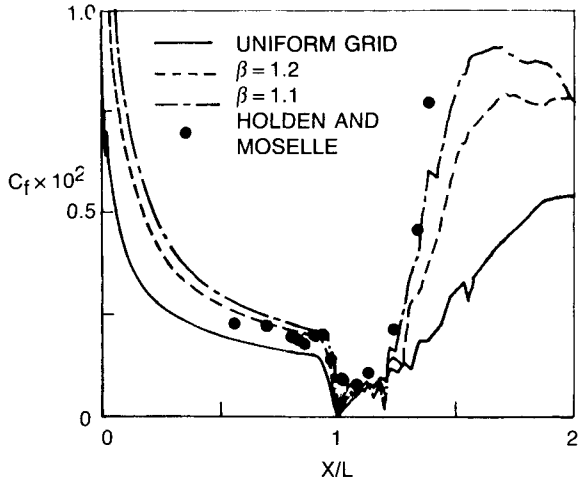

Fig. 4 Effect of grid on calculated skin friction for 15-deg case.

Figure 7 shows the extent of the enhanced grid, the calculated pressure contours from the primary solution, and the calculated contours within the local enhancement region. The contour levels calculated on the refined grid do not vary significantly from the primary solution, indicating that the effect of the viscous flow on the inviscid flow has not been altered during the enhancement calculation. Figure 8 shows temperature profiles for the primary and locally enhanced solutions at a location just upstream of the separation zone and at a location just downstream of the reattachment. The upstream profiles calculated on the primary and refined grids are described by 17 and 53 points, respectively, from the surface up to the point of maximum static temperature. On the other hand, the downstream profiles are described by only 3

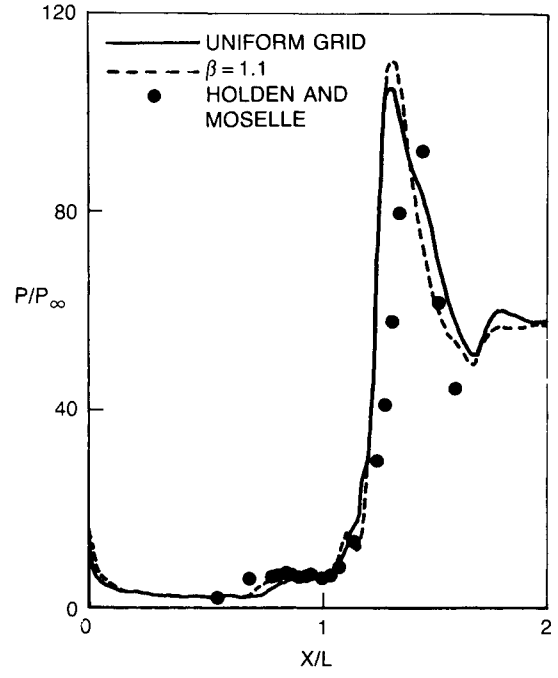

Fig. 5 Comparison of wall pressure distributions calculated on two grids for 24-deg case.

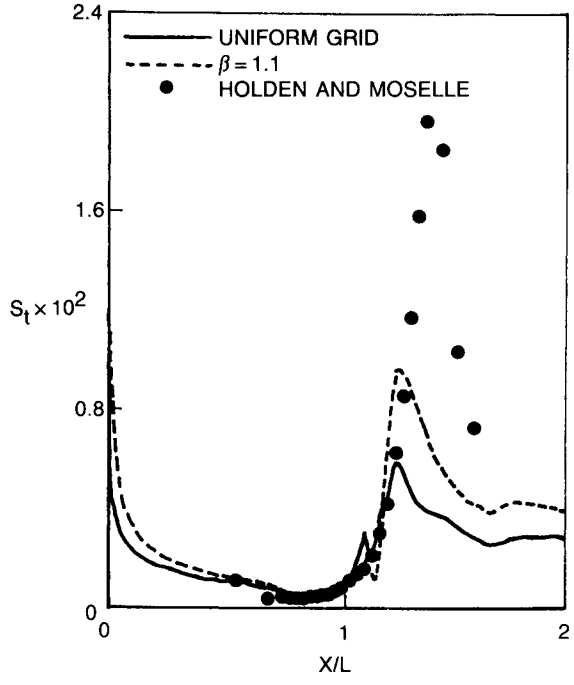

Fig. 6 Comparison of Stanton numbers calculated on two grids for 24-deg case.

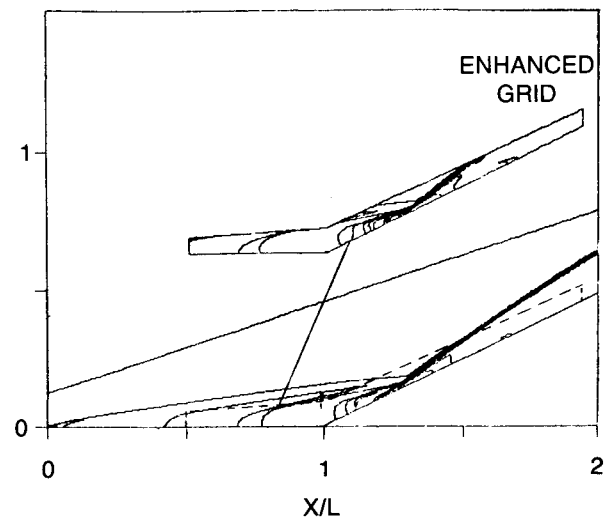

Fig. 7 Comparison of pressure contours calculated on the primary and enhanced computational grids (24-deg case).

Table 1 Efect of local enhancement approach on CPU

Case: flat plate/24 deg compression ramp	
Grid	CPU min (Alliant FX-8)
primary solution	1600.0
enhanced solution	500.0
total	2100.0
fine grid	>6400.0 (est.)

points in the primary flow calculation and by 6 points in the enhanced calculation. This figure further illustrates that the local enhancement has not affected the outer inviscid flowfield but has modified the inner viscous region, particularly downstream of attachment, where the grid was insufficient in the primary calculation. The Stanton number distributions for the primary and enhanced solutions are coplotted with the experimental data in Fig. 9. The predicted peak heat transfer obtained using the enhancement procedure is now adequately resolved and is in agreement with the data. The upstream shift of the peak compared to the measured results is similar to the shift seen in the pressure results.

Table 1 presents a comparison of the relative computational time required for a calculation on the coarse primary grid as well as the time required for the refined grid calculation. An estimate also has been made of the time required for a calculation on a grid fine enough to resolve accurately the inner viscous layer and the outer inviscid flow simultaneously (200×200). These times are based on calculations performed on the UTRC Alliant FX-8 vector/parallel computer. Although the local enhancement approach adds 30% to the time required for calculation on the primary grid, the total time required for both the primary and enhanced calculations is only a third of the estimated time required for calculation on a primary grid, with the same resolution as the enhanced grid. These results demonstrate that this method provides a more computationally efficient means for accurately calculating heat loads and drag penalties for hypersonic configurations without modifications to existing solution algorithms.

It is clear from an examination of the computational times presented in Table 1 that the NS method represents an expensive and time-consuming approach for use as a design tool. A more efficient approach is to use a spatially marching PNS method. Using this method, the resolution of the surface transport properties can be addressed by increasing the

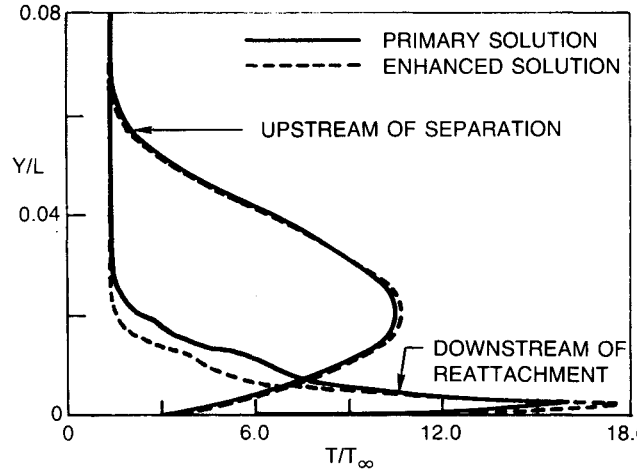

Fig. 8 Comparison of static temperature profiles calculated on the primary and enhanced grids.

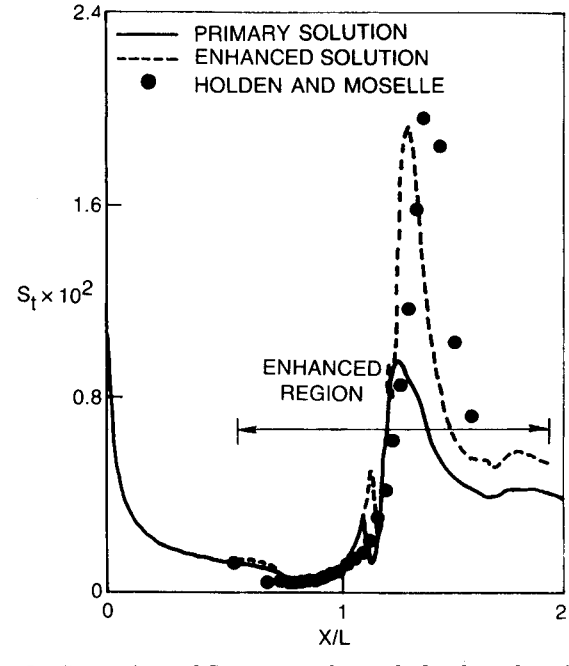

Fig. 9 Comparison of Stanton numbers calculated on the primary and enhanced computational grids (24-deg case).

number of points within the boundary layer without significantly degrading the efficiency of the computation. The SCRAMP PNS code was applied to the 24-deg configuration, with 75 points from the wall to the outer shock and 865 points in the axial direction. Points were clustered near the wall in the normal direction and near the leading edge and the corner in the axial direction. The axial step size distribution was based on stability and accuracy considerations. The leading-edge radius was specified to be 0.2% of the flat plate length so that the effects of the nose bluntness were limited to the near-nose region. The initial solution plane was obtained from a viscous shock-layer (VSL) solution[18] on the blunt leading edge.

Figure 10 is a plot of pressure distribution along the wall calculated by both the PNS and local enhancement NS procedures compared with the measured data. The NS results discussed earlier show a pressure rise to a plateau in the reversed flow region upstream of the corner. The PNS calculation, however, shows no pressure rise until the corner is reached, which indicates an inability to predict strong streamwise interaction. The skin-friction results shown in Fig. 11 also show large differences between the PNS and NS calculations within

and downstream of the strong interaction region. These results indicate that an RNS solution scheme would be appropriate to improve the PNS method by introducing the proper elliptic effects.

Upstream Influence

The most important difference between NS or RNS procedures and PNS procedures is that PNS methods exclude the prediction of strong streamwise interaction. Therefore, by comparing results from calculations made with an NS or RNS scheme and a PNS scheme, a qualitative understanding of the effect of upstream influence on the flowfield can be determined. The PNS solutions described next were calculated using the shock-fitting SCRAMP code, with 75 points across the flow and 590 points in the axial direction. As in the previously discussed PNS calculations, points were clustered near the wall in the normal direction and near the leading edge and the corner in the axial direction. The initial solution plane was obtained from a VSL solution on a blunt leading edge, with a radius of 0.2% of the flat plate length.

The pressure distributions calculated by the PNS, NS, and RNS methods are shown in Fig. 12 for the 15-deg configuration. The RNS solution was obtained on the same grid as the PNS solution but was globally iterated over a region that included 100 axial points from just upstream of the corner to a point downstream of the corner, as indicated in Fig. 12. Less than 50 iterations were required to converge the solution. Both the NS and RNS solutions indicate the upstream propagation of pressure information, although the strong streamwise interaction region is quite small for this attached-flow case. The PNS solution, however, shows no pressure rise until the corner is reached. Since the elliptic behavior is very localized, the effect on the overall pressure distribution is small.

Figure 13 shows the calculated values of skin friction compared with data for each algorithm. The PNS procedure predicts no reduction in skin friction prior to the corner, whereas the RNS solution indicates a substantial decrease that compares well with the NS solution and the experimental data in the immediate vicinity of the corner. One physical explanation of this effect is that the flow "feels" the disturbance through the upstream propagation of pressure waves in the subsonic portion of the boundary layer before the effects of the density variation across the shock on the boundary-layer thickness are felt. Thus, the adverse pressure gradient causes a reduction in skin friction before the thinning boundary layer induces an increase in skin friction downstream of the corner. Since the PNS solution has no mechanism for propagating this information upstream, the thinning boundary layer and the adverse gradient occur simultaneously, so that only a skin-friction rise is predicted. The effect of upstream influence on skin friction is not just local as in the pressure distribution but continues well downstream. This same effect downstream of the corner can be seen with heat transfer, as shown in Fig. 14, although not as dramatically. The most important difference between the NS and RNS calculations is seen in a comparison

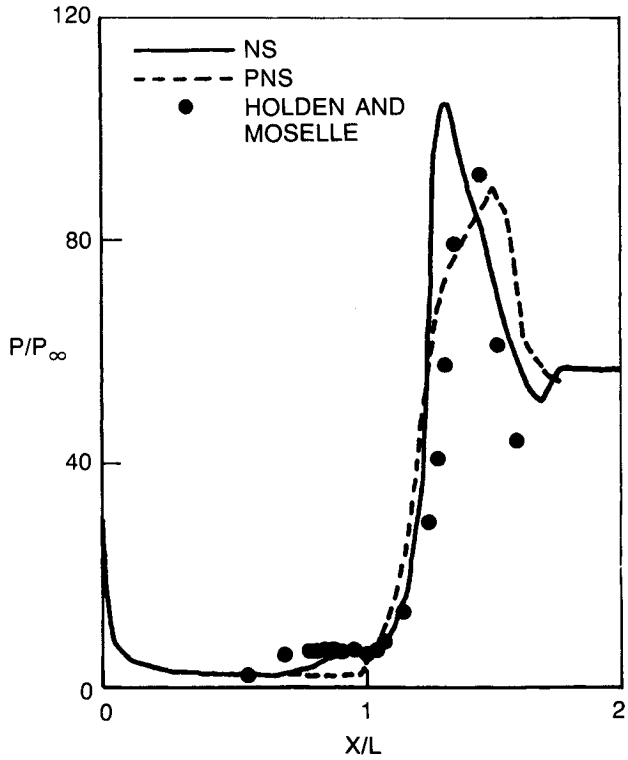

Fig. 10 Comparison of wall pressure distributions calculated using NS and PNS procedures (24-deg case).

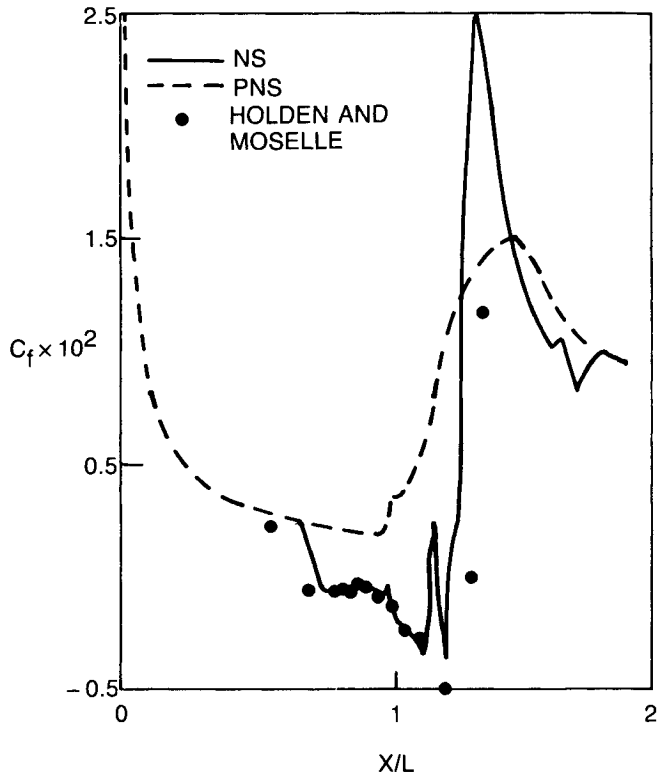

Fig. 11 Comparison of skin friction calculated using NS and PNS procedures (24-deg case).

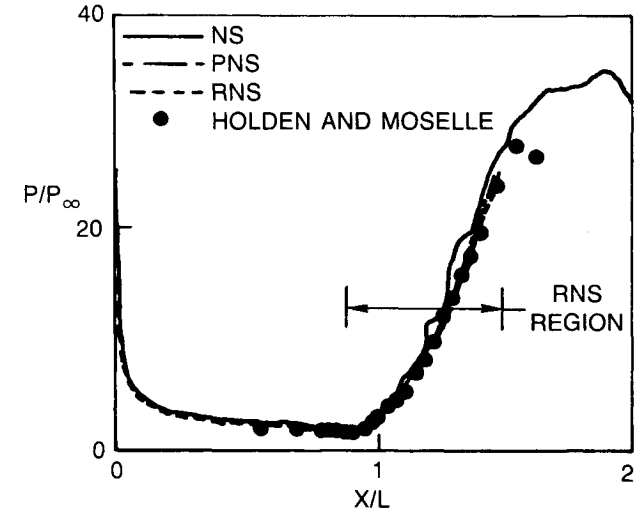

Fig. 12 Comparison of wall pressure distributions calculated using NS, PNS, and RNS procedures (15-deg case).

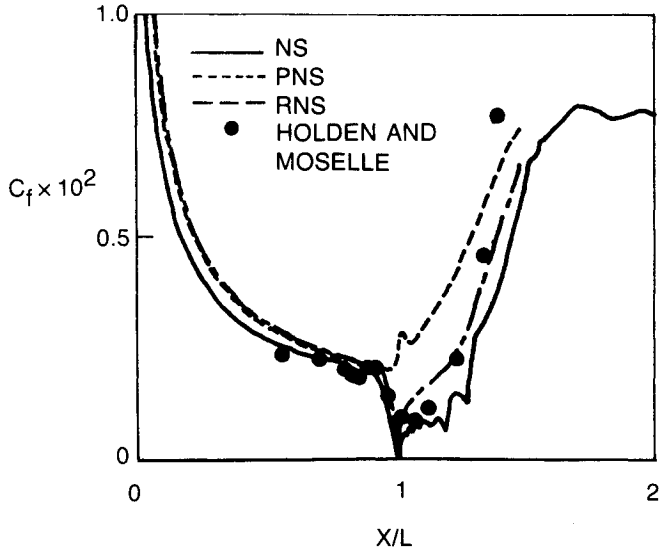

Fig. 13 Comparison of skin friction calculated using NS, PNS, and RNS procedures (15-deg case).

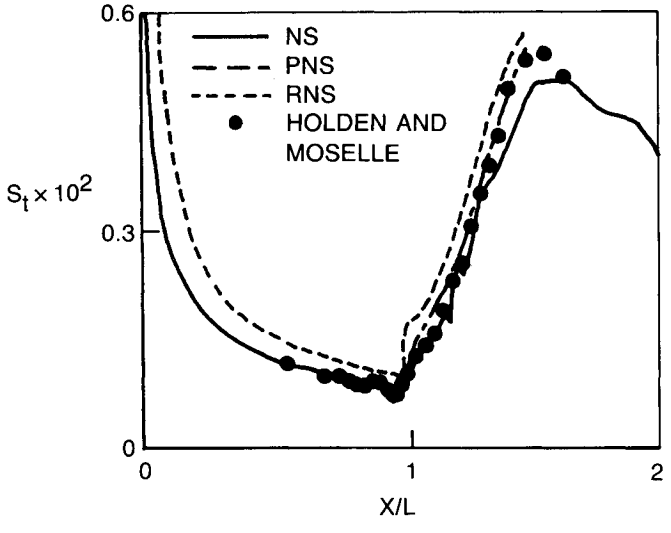

Fig. 14 Comparison of Stanton numbers calculated using NS, PNS, and RNS procedures (15-deg case).

of the computational effort; a factor of over 70 improvement was realized for this case by the RNS procedure compared to the NS algorithm, as shown in Table 2, which is a comparison of the relative computational effort required by the NS, PNS, and RNS schemes. The number of iterations required to converge an RNS calculation is strongly dependent on the extent of the interaction region, as described in Ref. 14.

Concluding Remarks

Due to the severe Mach number and altitude conditions at which hypersonic vehicles are expected to operate, computational fluid dynamics (CFD) will be required to predict thermal and pressure loads in the design of such a system. These vehicles and their associated propulsion systems are dominated by strong viscous/inviscid interactions, which must be computationally resolved to provide accurate predictions. In this study, the ability of current CFD analyses to compute hypersonic viscous/inviscid interaction and two methods to improve the efficiency and accuracy of these methods were addressed.

The results of the present study indicated that an explicit full Navier-Stokes (NS) solution method provided good comparisons with measured pressure data if there were sufficient resolution of the viscous and inviscid flowfields. However, the CPU and storage requirements increased as the grid was refined near the wall to accurately predict the surface transport properties. A more efficient computational procedure was proposed to resolve these gradients. In this procedure, the solution was obtained on a grid sufficient to accurately determine the pressure field but not necessarily the surface normal gradients. This solution then was used as the starting solution and boundary conditions for an ex post facto calculation on an enhanced grid incorporating only the near-wall region. It was found that accurate heat-transfer predictions could be obtained in this manner more efficiently than through calculation on a initial fine grid.

Table 2 Effect of solution scheme on CPU

Case: flat plate/15-deg compression ramp	
Algorithm	CPU min (Alliant FX-8)
PNS	2.85
RNS	12.0
NS	846.5

A parabolized Navier-Stokes (PNS) solution method, although very efficient due to its single-pass, space-marching approach, could not accurately predict flows with strong viscous/inviscid interaction (upstream influence) due to the nature of the solution algorithm. A modified form of this algorithm, known as reduced Navier-Stokes (RNS), allows the upstream propagation of information within the subsonic layer through a global pressure iteration approach. The results obtained using this method indicated good agreement with the NS solutions and with the measured heat-transfer data at a substantially reduced computational cost compared to the NS calculation.

Acknowledgments

The authors would like to acknowledge United Technologies Research Center, Pratt and Whitney, and the National Aerospace Plane program office for their support of this effort. Appreciation is also expresssed to Dr. M. S. Holden for providing his guidance and the data bases used in this study. Special note should be made of Dr. M. Barnett for his formulation and implementation of the global pressure iteration procedure for the SCRAMP code.

References

[1]MacCormack, R. W., "The Effect of Viscosity in Hypervelocity Impact Cratering," AIAA Paper 69-354, May 1969.

[2]Steger, J. L., "Implicit Finite-Difference Simulation of Flow About Arbitrary Two-Dimensional Geometries," *AIAA Journal,* Vol. 16, July 1978, p. 679.

[3]Schiff, L. B. and Steger, J. L., "Numerical Simulation of Steady Supersonic Viscous Flow," AIAA Paper 79-0130, Jan. 1979.

[4]Vigneron, Y. C., Rakich, J. V., and Tannehill, J. C., "Calculation of Supersonic Viscous Flow over Delta Wings with Sharp Supersonic Leading Edges," AIAA Paper 78-1137, July 1978.

[5]Barnett, M. and Davis, R. T., "A Procedure for the Calculation of Supersonic Flows with Strong Viscous-Inviscid Interaction," AIAA Paper 85-0166, Jan. 1985.

[6]Smith, F. T., "On High Reynolds Number Theory of Laminar Flows," *IMA Journal of Applied Mathematics,* Vol. 28, 1982, pp. 207-281.

[7]Carter, J. E., "A New Boundary Layer Interaction Technique for Separated Flows," AIAA Paper 79-1450, July 1979.

[8]Kumar, A., "Numerical Simulation of Scramjet Inlet Flow Fields," NASA TP-2517, May 1986.

[9]Roberts, G. O., "Computational Meshes for Boundary Layer Problems," *Lecture Notes in Physics,* Springer-Verlag, New York, 1971, pp. 171-177.

[10]Krawczyk, W. J., Rajendran, N., Harris, T. B., York, B. J., and Dash, S. M., "Computational Models for the Analysis/Design of

Hypersonic Scramjet Components—Part II," AIAA Paper 86-1596, June 1986.

[11]Tannehill, J. C. and Mugge, P. H., "Improved Curve Fits for the Thermodynamic Properties of Equilibrium Air Suitable for Numerical Computation Using Time-Dependent or Shock-Capturing Methods," NASA CR-2470, 1974.

[12]Atta, E. H. and Vadyak, J. A., "Grid Interfacing Zonal Algorithm for Three-Dimensional Transonic Flows About Aircraft Configurations," AIAA Paper 82-1017, June 1982.

[13]Rai, M. M., "A Conservative Treatment of Zonal Boundaries for Euler Calculations," AIAA Paper 84-0164, Jan. 1984.

[14]Barnett, M. and Power, G. D., "An Efficient Algorithm for Strong Viscous/Inviscid Interaction in Hypersonic Flows," AIAA Paper 88-0712, Jan. 1988.

[15]Holden, M. S. and Moselle, J. R., "Theoretical and Experimental Studies of the Shock Wave-Boundary Layer Interaction on Compression Surfaces in Hypersonic Flow," Calspan Corp., Buffalo, NY, CALSPAN Rept. AF-2410-A-1, Oct. 1969.

[16]Hung, D. M. and MacCormack, R. W., "Numerical Solutions of Supersonic and Hypersonic Laminar Compression Corner Flows," *AIAA Journal*, Vol. 14, April 1976, pp. 475–481.

[17]Lawrence, S. L., Tannehill, J. C., and Chaussee, D.S., "An Upwind Algorithm for the Parabolized Navier-Stokes Equations," AIAA Paper 86-1117, May 1986.

[18]Holcomb, J. E., Curtis, J. T., and Shope, F. L., "A New Version of the CVEQ Hemisphere Viscous Shock Layer Program for Equilibrium Air," Arnold Engineering Development Center, Arnold Air Force Station, TN, AEDC-TMR-85-V7, Feb. 1985.